A soil column model for predicting the interaction between water table and evapotranspiration

Mathilde Maquin, Emmanuel Mouche, Claude Mügler, Marie-Claire Pierret, Daniel Viville

AGU PUBLICATIONS

Water Resources Research

RESEARCH ARTICLE
10.1002/2016WR020183

A soil column model for predicting the interaction between water table and evapotranspiration

Mathilde Maquin[1], Emmanuel Mouche[1], Claude Mügler[1], Marie-Claire Pierret[2], and Daniel Viville[2]

[1]Laboratoire des Sciences du Climat et de l'Environnement, LSCE/IPSL, CEA-CNRS-UVSQ, Université Paris-Saclay, Gif-sur-Yvette, France, [2]Laboratoire d'Hydrologie et de Géochimie de Strasbourg, EOST, Université de Strasbourg/CNRS, Strasbourg, France

Key Points:
- This paper presents a hillslope-based column model (1-D) for modeling the soil-vegetation-atmosphere continuum
- The temporal evolution of the water table depth and its influence on the vegetation is taken into account through a drainage function
- The results of the model are in good agreement with 2-D simulations and with piezometers data (Strengbach catchment, France)

Correspondence to:
E. Mouche,
emmanuel.mouche@lsce.ipsl.fr

Citation:
Maquin, M., E. Mouche, C. Mügler, M.-C. Pierret, and D. Viville (2017), A soil column model for predicting the interaction between water table and evapotranspiration, *Water Resour. Res.*, *53*, 5877–5898, doi:10.1002/2016WR020183.

Received 25 NOV 2016
Accepted 25 JUN 2017
Accepted article online 5 JUL 2017
Published online 22 JUL 2017

Abstract Lateral waterfluxes are not realistically taken into account in soil column models, although they influence the dynamic evolution of the vertical soil moisture profile. By neglecting these fluxes, the modeling of the soil-vegetation-atmosphere continuum is incomplete, and the feedbacks between these three compartments cannot be fully simulated. These fluxes have an importance in the different fields where soil column models are used: hydrology, hydrometeorology, biogeochemical cycles, ecology, and soil weathering. This paper introduces a novel Hydrological Hillslope-based Soil Column model (H2SC) that simulates the temporal evolution of the water table depth and evapotranspiration fluxes and their interaction. The interconnected processes are infiltration, evapotranspiration, vertical soil water movements, and the non-explicitly modeled lateral fluxes flowing through the soil column. These lateral fluxes are modeled as a drainage function built from physically based equations that describe a simplified hillslope hydrology. This drainage function can be easily implemented in any soil column model without penalizing computational times. The H2SC model was validated on numerical experiments where a 2-D hillslope simulation performed with an integrated hydrologic model was compared with simulations using the H2SC 1-D model. Each of the H2SC simulations represents a specific location of a soil column along the hillslope. Different climate forcings, soil properties, and geometric shapes of the hillslope were tested. The model was then applied at the locations of two piezometers in the Strengbach catchment, France. The model reproduced the temporal evolution of the water table level fairly well for both the numerical experiments and for the real test case.

1. Introduction

The spatial and temporal evolution of soil water content is interconnected with land surface processes and vegetation dynamics [*Rodriguez-Iturbe et al.*, 2001; *Chen et al.*, 2015; *Ford et al.*, 2015]. All of the hydrological processes involving water flows depend on the soil water content profile and also influence it. On one hand, temporal and spatial variations in water content and atmospheric parameters drive the dynamic growth of vegetation and its temporal and spatial patterns. On the other hand, vegetation processes, which depend on the morphological features of the vegetation, impact the soil and the atmospheric water cycle. A good comprehension of the coupling which occurs at different spatial scales, from the plot to the watershed, between atmosphere, vegetation dynamics, and hydrological processes is important in different fields such as hydrometeorology, ecology, biogeochemical cycles, geochemistry of soil, and rock weathering. For example, a realistic representation of this coupling is necessary to address the following issues: the impacts of arid or semiarid climates on vegetation and soil erosion [*Rodriguez-Iturbe et al.*, 2001], the circulation of chemical nutrients in the soil (C, N, ...) and the weathering of soil and rock minerals [*Zhang et al.*, 2002; *Goddéris et al.*, 2009], the impacts of the climate change on vegetation or water resources, from the local to the regional scale [*Krinner et al.*, 2005; *Xia and Shao*, 2008], the measures to propose to stakeholders for forest and water management [*Chen et al.*, 2015]. Therefore, a hydrological model that incorporates vegetation and land surface processes is needed to accurately model at the different scales of interest the interactions and the feedbacks between atmospheric, vegetation, and water dynamics along the vertical soil-vegetation-atmosphere continuum and over time.

Models developed in the different scientific fields previously mentioned aim to represent the links between the biosphere, the soil hydrology, the climatic forcing, and their impacts on biogeochemical processes. They

describe transfers in the soil-vegetation-atmosphere continuum [*Zhang et al*., 2002; *Goddéris et al*., 2009; *Krinner et al*., 2005; *Chen et al*., 2015], and most of the processes involve vertical water transfers. Hence, the majority of these models represent only a soil column, e.g., Orchidée [*Krinner et al*., 2005], Noah-MP [*Niu et al*., 2011], VIC [*Liang et al*., 1994], and CLM [*Dai et al*., 2003]. The classical configuration of these models includes a free drainage at the bottom, as in Orchidée [*de Rosnay et al*., 2002], Noah [*Mahrt and Pan*, 1984], and ISBA [*Decharme et al*., 2011]. These models neglect by construction the lateral water transfers and the associated transport of chemical elements that occur through the soil column. However, the soil water content profile depends on the subsurface characteristics such as the spatial relationship to the groundwater table, or lateral subsurface flow. As a consequence, these column models are not able to take into account a potential near-surface water table flowing from hilltops to streams in a watershed, whereas the variations in the water table depth over time may impact significantly the soil water content in a column. Moreover, the space and time evolution of the water table level is jointly governed by topographic gradients and also by vegetation and land surface processes such as rainfall infiltration and root water uptake. This complex coupling induces feedbacks on atmospheric and vegetation processes. For instance, a shallow water table influences evapotranspiration fluxes by sustaining capillary rise [*Yeh and Eltahir*, 2005; *Kollet and Maxwell*, 2008; *Miguez-Macho and Fan*, 2012], as has been numerically observed [*Maxwell and Kollet*, 2008; *Condon et al*., 2013]. Simulations reveal that up to 20% of evapotranspiration can be drawn from an aquifer [*York et al*., 2002]. This coupling essentially concerns lowland areas, i.e., areas with shallow groundwater tables [*Brauer et al*., 2014a], which represent a significant part of the world [*Miguez-Macho and Fan*, 2012; *Fan et al*., 2013; *Brauer et al*., 2014a]. The extent and distribution of lowland area changes over time depend on the hydrological response of the catchment to seasons and climate. Hence, the catchment hydrology is also important to identify where these couplings between land surface processes, vegetation and water table occur. For example, feedbacks on climate can be induced by the increase of water transfers from the soil to the atmosphere due to a near-surface water table [*York et al*., 2002; *Anyah et al*., 2008; *Yuan et al*., 2008; *Jiang et al*., 2009; *Leung et al*., 2011; *Campoy et al*., 2013; *Vergnes et al*., 2014] as well as feedbacks on vegetation dynamics [*Fernandez-Illescas and Rodriguez-Iturbe*, 2003; *Ridolfi et al*., 2006; *Liu et al*., 2012]. As a consequence, the representation of shallow groundwater is of particular importance to properly model soil-vegetation-atmosphere interactions and their impact on biogeochemical cycles and soil weathering processes. Integrated hydrologic models coupled to land surface models offer this possibility, e.g., Parflow with CLM [*Maxwell and Miller*, 2005], Cathy with NoahMP [*Niu et al*., 2014], Modflow with Vos [*York et al*., 2002]. Other hydrological models directly include the vegetation and land-surface processes, such as HydroGeoSphere [*Li et al*., 2008] or Amanzi-ATS [*Coon et al*., 2016]. However, the implementation of these codes is complex. The objective of the present paper is to propose a simpler model that relies on the soil column concept. In soil column models, whatever their application, the water table is generally assumed to be too deep to interact with the vegetation [*Rodriguez-Iturbe et al*., 2001; *Xia and Shao*, 2008]. Only the vertical water transfers in the unsaturated zone are taken into consideration. The question of how to incorporate lateral hydrological processes into vertical column models has been emphasized in the literature [*Chen et al*., 2015].

An option for introducing groundwater flow in column models is to couple columns with a 2-D or 3-D groundwater model. This has been done by different authors and tested on various test cases and at different spatial scales. One can cite *Twarakavi et al*. [2008] and *Niswonger et al*. [2006] who performed a coupling between HYDRUS 1-D and MODFLOW softwares, or *Zhu et al*. [2012] who proposed a coupling strategy devoted to regional studies. The coupling between SVAT models, based on soil column models, and discretized hydrogeological models must be also mentioned, e.g., MIKE SHE [*Graham and Butts*, 2005] or SIM [*Habets et al*., 2008]. However, this option has a cost in terms of numerics and computing time: the Darcy equations must be discretized on a 2-D or 3-D mesh and coupled with the Richards equation in each column.

Taking into account the specificities of catchment hydrology, *Hazenberg et al*. [2015, 2016] have recently proposed a hillslope model that couples the vertical resolution of the Richards equation with the lateral resolution of a Boussinesq equation. Following the work of *Troch et al*. [2003], this last equation is reformulated in terms of soil water storage and denoted HsB equation. The resulting model (h3D) is designed to simulate the runoff of a hillslope without solving the Richards equation in the whole hillslope. However, a simpler column model based on a drainage equation would lead to reduced calculation times and would be

coherent with the level of simplifications generally introduced in column models to describe processes such as water uptake by the roots, weathering processes, nutrient migration. This paper addresses this issue: how to incorporate in a soil column model a drainage function at the bottom of the column that represents in a simple but realistic way the spatial and temporal evolution of a water table in interaction with vegetation and atmospheric processes?

In the present paper, we describe a new Hydrological Hillslope-based Soil Column model (denoted H2SC) for coupling the vegetation cover and its root profiles with the water table dynamics. This model is based on a physical approach in the vertical direction and on a simplified description of the complex 3-D saturated flow in the other directions. A drainage function is added to represent the lateral water transfers in the saturated zone. The function is built from physically based equations of a simplified hydrological behavior at the hillslope scale. The hillslope scale was chosen as the basic unit of the hydrological part of the H2SC model because this scale is recognized as a meaningful and fundamental hydrologic unit [*Carrillo et al*., 2011; *Miguez-Macho and Fan*, 2012; *Hazenberg et al*., 2015].

We first describe the approach and explain in detail the structure of the H2SC model and the equations used (section 2). The evaluation of the model on synthetic test cases is presented in section 3, and its application to the Strengbach catchment (France) is discussed in section 4. The conclusions are presented in the last section.

2. H2SC 1-D Vertical Column Model

2.1. Representation of a Hillslope

The H2SC model represents a soil column that must be associated with the hillslope it belongs to in the catchment. In a catchment, streamlines behave as impermeable limits [*Bear*, 1972; *Fan and Bras*, 1998]. Therefore, water flows in the streamline system are 2-D. The streamline that intersects the location of the modeled soil column is used to define the "hillslope" needed for the model. This hillslope may be approximated by the steepest slope from the hilltop of the catchment to the stream that intersects the location of the soil column. The hillslope is described by its geometry, its soil type and its vegetation, all of which are supposed to be homogeneous. The rainfall is also assumed to be uniform. The geometric parameters are the length of the hillslope, L_t, the aquifer height below the river, h_r, the aquifer slope, α, and the surface slope, γ, as shown in Figure 1a. The soil column is then characterized by its distance to the river, L.

The soil and vegetation types in the column are the same as those assigned to the hillslope. The height of the column, Δh, is equal to the thickness of the hillslope at the distance L from the river (Figure 1a):

$$\Delta h = h_r + L(\tan\gamma - \tan\alpha). \quad (1)$$

The associated boundary conditions for the hillslope are as follows. The upslope end of the hillslope represents a watershed divide. Hence, it corresponds to a no-flow boundary condition, such as the lower surface

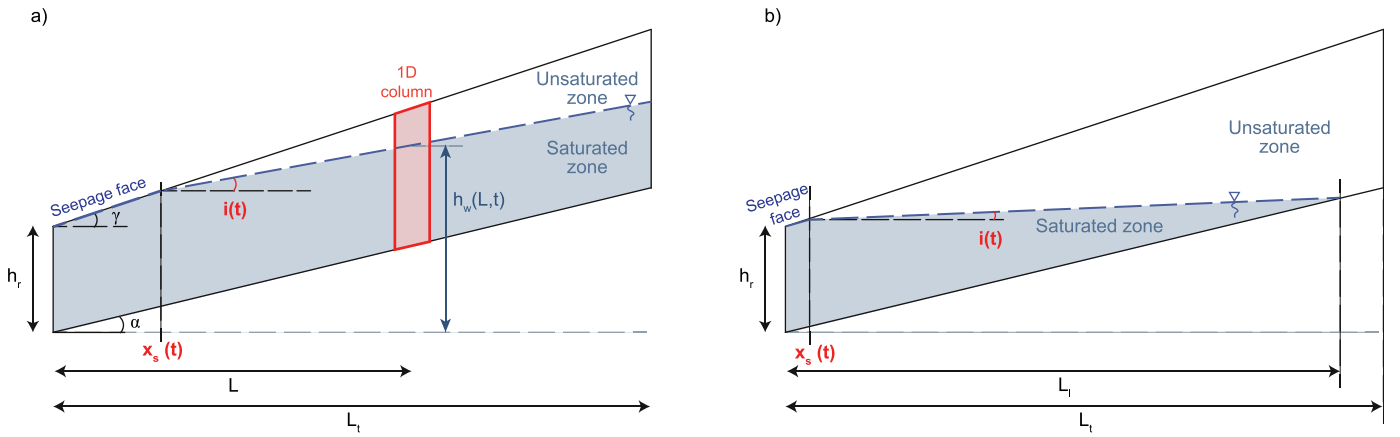

Figure 1. Schematic representation of an idealized hillslope and of the selected column: (a) case where the water table level does not intersect the bedrock, (b) case where the water table intersects the bedrock and definition of the parameter L_l.

delineating an impermeable layer. A specified head boundary condition is employed at the downslope end to represent the river [*Ogden and Watts*, 2000].

2.2. Vertical Flow Through the Soil Column

Surface and subsurface flows are modeled by the generalized Richards type equation developed by *Weill et al*. [2009]. The resolution of this equation is limited to the vertical dimension for the H2SC model. This equation unifies the surface and subsurface flow equations by using domain-dependent parameters. It allows the surface and subsurface flow equations to be solved in a single domain instead of introducing an interface with a change in the boundary conditions.

In the subsurface domain, the generalized equation is equivalent to the Richards equation:

$$\sigma(h)\frac{\partial h}{\partial t}-\vec{\nabla}\cdot\left(K(h)\vec{\nabla}(h+e_s-z)\right)+d(z,t)+ev(z,t)+tr(z,t)=0, \tag{2}$$

where h is the pressure head [L], t is time [T], z is the depth [L], e_s is the soil elevation [L], $\sigma(h)$ is the specific volumetric storativity [L^{-1}], $K(h)$ is the hydraulic conductivity [LT^{-1}], d is the drainage uptake [T^{-1}] (section 2.4), and ev and tr are the evapotranspiration uptake of water [T^{-1}] (section2.3).

In the surface domain, the generalized equation is equivalent to the diffusive-wave approximation of the Saint Venant equation associated with the Manning-Strickler flow formula. The details are outlined in *Weill et al*. [2009].

2.3. Vegetation Model

The vegetation model is based on the Orchidée land surface model [*de Rosnay and Polcher*, 1998]. It accounts for evaporation from bare soil, transpiration by root water uptake and interception loss, which is the evaporation of the intercepted rainfall by the foliage. The soil-plant interaction is modeled using a macroscopic approach, i.e., the root system is represented as a diffuse sink that is uniform in each layer but may vary with depth [*Feddes et al*., 2001]. The foliage is represented by the "big-leaf" approach, i.e., the vegetation cover is simplified by considering a single leaf [*de Rosnay*, 1999]. Only one type of vegetation can be prescribed for a column of the H2SC model.

The transpiration flux $TR(t)$ is computed at each time step by integrating the root water uptake in each layer of the root zone $tr(z,t)$:

$$TR(t)=\int_0^{z_{\max}} tr(z,t)dz, \tag{3}$$

where $z_{\max}$ is the limiting depth of the root zone, z is the depth, and t is the time. The root water uptake at a given depth depends on the potential evapotranspiration E_p, the fraction of soil covered by the vegetation, the fraction of foliage that is not covered by intercepted water, a resistance term $f_{r1}(t)$, the water availability $g_t(\theta)$, and the root density $h_t(z)$:

$$tr(z,t)=E_p(1-f_{bs})\left(1-\frac{I}{I_{\max}}\right)f_{r1}g_t(\theta)h_t(z), \tag{4}$$

where f_{bs} is the fraction of bare soil inside the vegetation cover, I is the amount of water intercepted by the foliage, and $I_{\max}$ is the maximal amount of water the foliage may intercept. The expressions of these variables can be found in Appendix A.

The evaporation, $EV(t)$, is calculated applying a similar methodology:

$$EV(t)=\int_0^{z'_{\max}} ev(z,t)dz, \tag{5}$$

where $z'_{\max}$ is the limiting depth for the evaporative uptake, and z is the depth. It is assumed that the evaporative uptake occurs over a specific thickness due to energy penetration in the soil. The water uptake for evaporation, $ev(z,t)$, is proportional to the potential evapotranspiration, the fraction of bare soil, a water availability function for evaporation, $g_e(\theta)$, and an evaporation distribution function, $h_e(z)$, that represents the reduction of energy penetration in the soil. The total water uptake from evaporation, transpiration, and interception must be lower than the potential evaporation. As a consequence, $ev(z,t)$ is given by

$$ev(z,t)=\min\left(E_p,\ E_p f_{bs}-TR-IN\right)g_e(\theta)h_e(z). \quad (6)$$

2.4. Water Table Dynamics

The conceptual representation of the system under study is an unconfined aquifer flowing from a hilltop to the stream. In the H2SC model, the water table dynamics is modeled via a drainage uptake $d(L,z,t)$ that represents the total flow-rate through the column. The column is characterized by its distance to the river, L (Figure 1a). The drainage function is introduced as a sink term in the Richards equation (equation (2)) in the lowest layer of the column. The drainage uptake is linked to the drainage flux function, i.e., the flux of water extracted from the column, D [LT^{-1}], as follows:

$$D(L,t)=\int_z d(L,z,t)\mathrm{d}z. \quad (7)$$

The simulation of the whole hillslope is required to get the exact total flow rate through the column. Therefore, some simplifying assumptions are necessary to obtain an estimation of this flow rate. The adopted approach consists in establishing a drainage function from a simplified but physical hydrological behavior of the hillslope.

The groundwater level is supposed to be linear along the hillslope with a variable seepage face (Figure 1). This hypothesis of a linear water table is realistic for hillslopes with gentle and uniform soil slopes, with permeable and generally homogeneous soils and with a near-surface aquifer. In such cases, the water table responds almost instantaneously to a rainfall event throughout the entire hillslope, and the water table slope can be considered as constant. This assumption of a linear water table is also consistent with the hypothesis of a water table parallel to the topography in the TOPMODEL code [*Beven and Kirkby*, 1979]. Moreover, a linear water table is a simple approximation that has the advantage of introducing only two parameters (the slope and the intercept point). The use of a parabolic function to describe the water table level would be more realistic. However, it would lead to significant complications for the model because a third parameter should be introduced. To solve the resulting equation system, an additional relationship should be found and thus another physical assumption should be proposed. In the perspective of a simple and computational costless approach, the assumption of a linear water table provides a satisfying compromise between a simple but realistic representation of the water table level. This will be shown and discussed further in sections 3 and 4. Two variables define the groundwater level over space and time (Figure 1a): the angle with respect to the horizontal axis, $i(t)$, and the extension of the seepage face, $x_s(t)$. The groundwater level is defined as follows:

$$h_w(x,t)=\begin{cases} h_r+x\ \tan\ \gamma & \text{if } x\in[0;x_s] \\ h_r+x_s\ \tan\gamma+(x-x_s)\ \tan\ i & \text{if } x\in]x_s;L_l] \end{cases}, \quad (8)$$

where $h_w(x,t)$ is the water table level at a distance x from the river and at time t, h_r is the height of the aquifer below the river, and γ is the surface slope (Figure 1a). $L_l(t)$ is defined as the length of the hillslope, L_t, when the water table does not intersect the bedrock. Otherwise, L_l is the distance between the river and the location where the water table intersects the bedrock (Figure 1b):

$$L_l(t)=\begin{cases} \min\left(L_t,\ \dfrac{h_r+x_s(\tan\ \gamma-\tan\ i)}{\tan\alpha-\tan\ i}\right) & \text{if } i<\alpha \\ L_t & \text{if } i\geq\alpha \end{cases}. \quad (9)$$

The temporal evolutions between $t-dt$ and t of the two variables of this water table model, $i(t)$ and $x_s(t)$, depend on their respective values at time $t-dt$. Three different situations can occur at time t: (i) the groundwater level has decreased in the column ($h_w(t-dt)>h_w(t)$) and there was no seepage face at the previous time step ($x_s(t-dt)=0$), (ii) as in the previous case, except that the extension of the seepage face was positive ($x_s(t-dt)>0$), and (iii) the groundwater level has increased ($h_w(t-dt)<h_w(t)$). In the first case, we suppose that the water table level remains linear with a fixed level equal to h_r at the downstream point of the hillslope (Figure 2a). There will still be no seepage face at the next time step. This case represents a smooth discharge of the hillslope in the river. The greater the distance from the river, the more significant the decrease in the water level. In the second case, the water table is supposed to remain at a constant level at the distance L_l (Figure 2b). The extension of the seepage face decreases in this situation. This case represents a rapid discharge of the seepage face in the river. In this situation, the groundwater level remains

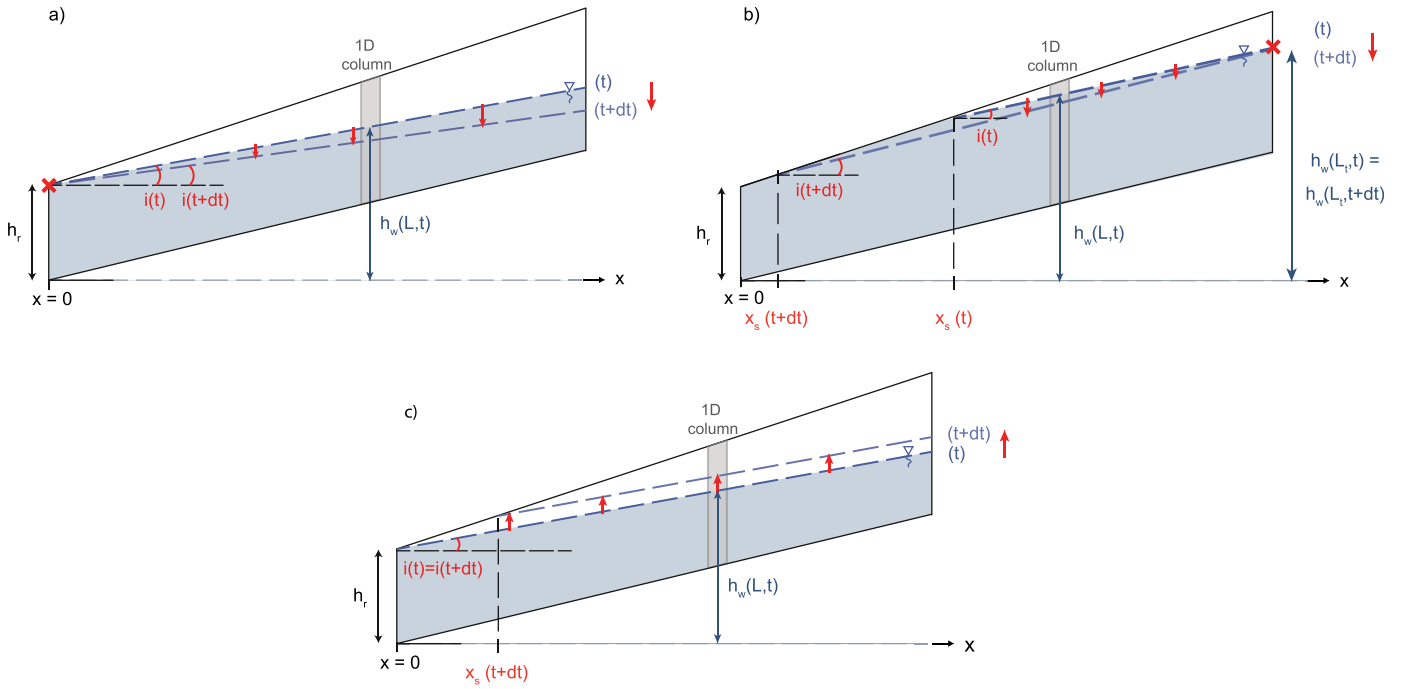

Figure 2. Representation of the three different cases for the evolution of the two variables $i(t)$ and $x_s(t)$ and: (a) the water table level is decreasing in the soil column, and there was no seepage face, (b) the water table level is decreasing in the soil column, and there was a seepage face, and (c) the water table level is increasing in the soil column.

almost constant far from the seepage face, and this justifies the hypothesis that the water table level does not evolve at the upstream point ($x=L_t$). Finally, the third case concerns a period where the water table rises in the column model. The infiltration time of the rainfall water amount in the unsaturated zone is assumed to be homogeneous along the hillslope and thus also the rise of the water table level (Figure 2c). This leads to the introduction and increase of the seepage face.

Finally, the drainage function for representing the lateral flow through the column based on these hypotheses is proposed as follows:

$$D(L,t)=\begin{cases} D_1+\Delta_{EV} & \text{if } x_s=0 \\ D_2+\Delta_{EV} & \text{if } x_s>0 \text{ and if } L\le L_s \\ (1-f_1(L_s))\times D_1+f_1(L_s)\times D_2+\Delta_{EV} & \text{if } x_s>0 \text{ and if } L>L_s, \end{cases} \tag{10}$$

where D_1 and D_2 are the two main drainage functions depending on whether there is a seepage face or not, respectively, and f_1 is a mixing function to ensure a smooth transition between the two drainage functions. Δ_{EV} is a function that accounts for the influence of the evapotranspiration fluxes on the water table dynamics. L_s, which is called the seepage-dominant distance, is a parameter that defines the transition between the case with no seepage face and the one with a seepage face.

In the following subsections, we describe the approach used to obtain these functions' members, and we specify their formulae. D_1, D_2, f_1, and L_s are described in section 2.4.1, and Δ_{EV} is introduced in section 2.4.2.

2.4.1. The Drainage Function Without Evapotranspiration Fluxes

The derivation of the drainage function (equation (10)) is based on a global water balance at the hillslope scale, a relationship between the variation of the volume of water in a column at a given distance of the river and the variation of the volume of water in the whole hillslope. Ignoring precipitation and evapotranspiration, which are modeled directly in the column, the water balance at the hillslope scale is

$$\frac{dV_w}{dt}+Q_{out}^{soil}+Q_{out}^{sf}=0, \tag{11}$$

where V_w is the volume of water in the hillslope, Q_{out}^{soil} is the flow of water through the downslope end, and Q_{out}^{sf} is the flow of water through the seepage face. These two flows are calculated using Darcy's law and equation (8):

$$\begin{cases} Q_{out}^{soil}(t) = \begin{cases} K_{sat} h_r \tan i & \text{if } x_s = 0 \\ K_{sat} h_r \tan \gamma & \text{if } x_s > 0 \end{cases} \cdot \\ Q_{out}^{sf}(t) = K_{sat} x_s (\tan \gamma)^2 \end{cases} \tag{12}$$

where K_{sat} is the saturated hydraulic conductivity [LT^{-1}].

Various relationships between the variation of the volume of water in the hillslope and in a column at a given distance from the river are established in the following sections for the different hydrological regimes that the model describes. Their relationships depend on the values of $L_l(t)$, $x_s(t)$, and $i(t)$.

2.4.1.1. No Seepage Face Case ($x_s(t)=0$)

First, we consider the particular case where there is no seepage face (Figure 2a). Furthermore, if $L_l(t)=L_t$, and $i(t) \neq \gamma$, there is a saturated zone and an unsaturated zone along the whole hillslope, and the following equation is established:

$$\frac{dV_w}{dt}(t) = \int_{x=0}^{L_t} \int_{z=h_w}^{h_r + x\tan\gamma} \frac{\partial \theta}{\partial t}(x,z,t)\mathrm{d}z \ \mathrm{d}x, \tag{13}$$

where θ is the soil moisture described by the van Genuchten function in the unsaturated zone [*van Genuchten*, 1980]. The pressure head, h, and the hydraulic head, H, are linked via the depth, z, and the soil elevation, e_s, as follows: $H=h+e_s-z$.

The assumption of a constant hydraulic head along a vertical profile and the time derivative of the van Genuchten function lead to

$$\frac{\partial \theta}{\partial t}(x,z,t) = -(\theta_s - \theta_r)\frac{\partial}{\partial z}\left(\left[1+(-\beta(h_w(x,t)-z))^n\right]^{-m}\right)\frac{\partial h_w}{\partial t}(x,t), \tag{14}$$

where β, n, and $m=1-1/n$ are empirical shape-defining parameters of van Genuchten, and θ_s and θ_r are the saturated and residual water contents, respectively.

Moreover, the water table is linear, and its value is imposed at a constant level at the river. One may then infer a relationship between the variations in the water table levels at two different distances from the river, x_1 and x_2:

$$\forall\ (x_1,x_2) \in [0;L_l]^2,\ \ \frac{\partial h_w}{\partial t}(x_1,t) = \frac{x_1}{x_2}\frac{\partial h_w}{\partial t}(x_2,t). \tag{15}$$

As a final step, we combine equations (13)–(15):

$$\frac{dV_w}{dt}(t) = \frac{(\theta_s-\theta_r)}{L}\frac{\partial h_w}{\partial t}(L,t)\left(\frac{L_t^2}{2} - \int_{x=0}^{L_t} x\left[1+(\beta x(\tan\gamma - \tan i))^n\right]^{-m}\mathrm{d}x\right), \tag{16}$$

where L is a given distance to the river (Figure 1a).

On the other hand, the variation in the volume of water in a given column at a distance L from the river is

$$\frac{dV_w^{col}}{dt}(L,t) = \int_{z=h_w}^{h_r + L\tan\gamma} \frac{\partial \theta}{\partial t}(z,t)\mathrm{d}z. \tag{17}$$

Using equations (14) and (17), we obtain

$$\frac{dV_w^{col}}{dt}(L,t) = (\theta_s-\theta_r)\frac{\partial h_w}{\partial t}(L,t)\left(1-\left[1+\beta^n(h_r+L\tan\gamma - h_w(L,t))^n\right]^{-m}\right). \tag{18}$$

As a final step, we combine equations (11), (16), and (18):

$$\frac{dV_w^{col}}{dt}(L,t) = -Q_{out}^{soil}\ L\ \frac{\psi}{\frac{L_t^2}{2}-\varphi_0}, \tag{19}$$

with

$$\psi(L,t)=1-\left[1+\beta^n\left(h_r+L\tan\gamma-h_w(L,t)\right)^n\right]^{-m}\text{and} \tag{20}$$

$$\varphi_0(t)=\int_{x=0}^{L_t} x\left[1+\left(\beta\ (\tan\gamma-\tan i)x\right)^n\right]^{-m}\mathrm{d}x. \tag{21}$$

This final equation corresponds to the "drainage function" for the case $x_s(t)=0$, $L_l(t)=L_t$, and $i(t)\neq\gamma$. The development of equation (19) into a Taylor series shows that this drainage function is still valid for $i(t)=\gamma$.

For the case $L_l(t)<L_t$, the drainage function is obtained by applying the same methodology. An additional and particular situation must be considered: when the distance L of the column to the river is larger than $L_l(t)$, i.e., the whole column is unsaturated. In that case, we apply a free drainage at the bottom of the column.

Finally, when $x_s(t)=0$, we obtain the following general expression for the drainage function, denoted $D_1(L,t)$:

$$D_1(L,t)=\frac{dV_w^{col}}{dt}(L,t)=\begin{cases}-Q_{out}^{soil}(n+2)\dfrac{L^{n+1}}{L_t^{n+2}} & \text{if } i=\gamma\\ -Q_{out}^{soil}\ L\ \dfrac{\psi}{\frac{L_l^2}{2}-\varphi_1} & \text{if } i\in\ ]i_l;\gamma]\ \text{or}\ (i<i_l\ \text{and}\ L<L_l)\\ K_{sat}k_r\left(h(z_{col}=0)\right) & \text{if } i<i_l\ \text{and}\ L\geq L_l\end{cases}. \tag{22}$$

In this expression, i_l is the water table angle such that the water table intersects the bedrock at $x=L_t$:

$$i_l(t)=\arctan\left(\frac{L_t\ \tan\alpha-x_s\ \tan\gamma-h_r}{L_t-x_s}\right). \tag{23}$$

The function $\varphi_1(t)$ in equation (22) is defined as follows:

$$\varphi_1(t)=\int_{x=0}^{L_l} x\left[1+\left(\beta x(\tan\gamma-\tan i)\right)^n\right]^{-m}\mathrm{d}x. \tag{24}$$

The drainage function, $D_1(L,t)$, and the flow of water through the downslope end of the hillslope, $Q_{out}^{soil}(t)$, have opposite signs. For $i(t)>0$, the flow through the downstream boundary condition is oriented outside of the hillslope, and the drainage function is negative. This leads to a fall in the water table level in a column, as expected. On the contrary, for $i(t)\leq 0$, the river contributes to the recharge of the aquifer, and the drainage function is positive.

2.4.1.2. Seepage Face Case ($x_s(t)>0$)

The same methodology as in the case with no seepage face is applied. In this case (Figure 2c), the drainage function is denoted $D_2(t)$. One may notice that the hypothesis concerning the evolution of the water table is different from the previous case. The water level is imposed at $x=L_l(t)$ instead of $x=0$. Equation (15) becomes

$$\forall\ (x_1,x_2)\in[x_s;L_l]^2,\ \frac{\partial h_w}{\partial t}(x_1,t)=\frac{L_l-x_1}{L_l-x_2}\frac{\partial h_w}{\partial t}(x_2,t). \tag{25}$$

It can then be shown that the drainage function D_2 is

$$D_2(L,t)=\begin{cases}-\left(Q_{out}^{soil}+Q_{out}^{sf}\right)(n+1)(n+2)\dfrac{(L_t-L)L^n}{(L_t-x_s)^{n+2}} & \text{if } i=\gamma\\ -\left(Q_{out}^{soil}+Q_{out}^{sf}\right)\dfrac{(L_l-L)\psi}{\frac{(L_l-x_s)^2}{2}-\varphi_2} & \text{if } i\in\ ]i_l;\gamma]\ \text{or}\ (i<i_l\ \text{and}\ L<L_l)\\ K_{sat}k_r\left(h(z_{col}=0)\right) & \text{if } i<i_l\ \text{and}\ L\geq L_l\end{cases}, \tag{26}$$

with

$$\varphi_2(t)=\int_{x=x_s}^{L_l}(L_l-x)[1+(\beta\ (\tan\gamma-\tan i)(x-x_s))^n]^{-m}\mathrm{d}x. \tag{27}$$

2.4.1.3. Transitional Case

To ensure a soft transition between the functions D_1 and D_2, a phase involving a combination of the two functions is introduced. The drainage function D_1 represents a discharge of the groundwater in the river, whereas D_2 corresponds to a fast discharge after a rainfall. This fast discharge is mainly due to the exfiltration of the water table along the seepage face. However, the impact of the seepage face is only significant in the seepage area. Beyond a given distance from the seepage face, which is denoted L_s and called the "seepage-dominant distance," the impact of the seepage face on the discharge decreases until the discharge of the groundwater in the river becomes dominant. To estimate L_s, we assume that the variation in the volume of water in the interval $x \in [x_s(t);L_s(t)]$ is equal to the flow of water through the seepage face, Q_{out}^{sf}. Then, the formulation of this hypothesis is

$$\int_{x=x_s}^{L_s}\frac{\partial V_w^{col}}{\partial t}(x,t)\ \mathrm{d}x=Q_{out}^{sf}(t). \tag{28}$$

Using the second case of equation (26) and approximating $\psi(x,t)$ by $\psi((x_s(t)+L_s(t))/2,t)$, we deduce that $L_s(t)$ is a solution of

$$g(X)=\left[\left(L_l(X-x_s)-\frac{X^2}{2}+\frac{x_s^2}{2}\right)\right]\left[1-\left(1+\left(\beta\frac{X-x_s}{2}(\tan\gamma-\tan i)\right)^n\right)^{-m}\right]-\frac{Q_{out}^{sf}}{Q_{out}^{soil}+Q_{out}^{sf}}\left(\frac{(L_l-x_s)^2}{2}-\varphi_2\right)=0. \tag{29}$$

The function $g(X)$ is strictly increasing over the interval $X \in]x_s;L_t]$, and $g(X=x_s)$ is negative. If $g(X=L_t)<0$, the equation $g(X)=0$ has no solution. The impact of the seepage face exceeds the length of the hillslope. If $g(X=L_t)\geq 0$, the equation has a unique solution, $L_s(t)$, which can be approximated by numerical methods. Finally, the "seepage-dominant distance" is given by

$$L_s(\mathrm{t})=\begin{cases}L_l & \text{if } g(X=L_l)\leq 0\\ \text{the unique solution of } g(X)=0 & \text{if } g(X=L_l)>0\end{cases}. \tag{30}$$

2.4.1.4. General Case

In summary, the global drainage function without a consideration of the evapotranspiration fluxes, $D(L,t)$, which models the water table dynamics in the column, is given by equation (10) with $\Delta_{EV}=0$, and where D_1 and D_2 are given by equations (22) and (26), respectively. In equation (10), f_1 is a mixing function defined for $L_s \in [0;L]$ such as $f_1(L_s=L)=1$. Moreover, the influence of the seepage face on the drainage drops to zero when the seepage face disappears, i.e., when $L_s(t)=0$. Then, $f_1(L_s=0)=0$. The chosen function is based on the arctangent function:

$$f_1(X)=\frac{1}{2}\left(1+\frac{2}{\pi}\arctan\left(-C\left(\frac{1}{X}+\frac{1}{X-L}\right)\right)\right), \tag{31}$$

where $C=-\tan(0.8\times\pi/2)/(1/X_0+1/(X_0-L))$, and $X_0=3L/4$, such as $f_1(X=X_0)=0.9$. The arctangent function has been chosen because its derivative is zero in $-\infty$ and $+\infty$. Consequently, the derivative of the function f_1 is 0 when $L_s=L$, that leads to a continuous transition between the transitional case and the case $D=D_2$. From a numerical point of view, a continuous transition prevents from oscillations between the two cases. Similarly, the derivative of f_1 is 0 when $L_s=0$ and the transition between the transitional case and the case $D=D_1$ is continuous. Moreover, the function f_1 is built so that the weight given to D_1 and D_2 is symmetric between the cases $L_s=X$ and $L_s=L-X$.

2.4.2. The Evapotranspiration Fluxes

The evaporation and transpiration fluxes are two sink terms in the water budget that pump some of the water near the surface and along the root zone, respectively. In the H2SC model, near the downstream boundary condition where the hydraulic head is fixed, the modeled river may contribute to these fluxes. This contribution has to be taken into account in the drainage function. We consider a flat hillslope for estimating this flow from the river. This initially flat water table would decrease uniformly along the hillslope if the hydraulic head was not imposed. In the case of an imposed groundwater level for modeling the river, we assume that the water table decreases while remaining linear. The configuration of this case is the same as for the determination of D_1 which is still available for a negative angle i.

In that specific case, the water balance at the hillslope scale must account for the evapotranspiration fluxes:

$$\frac{dV_w}{dt}+Q_{out}^{soil}-(Ev+Tr)\times L_t=0, \tag{32}$$

where Ev and Tr are the evaporation and transpiration fluxes, respectively. Moreover, the variation of the volume of water in a column must be updated as follows:

$$\frac{dV_w^{col}}{dt}(L,t)=D_1^{EV}(L,t)-(Ev+Tr), \tag{33}$$

where D_1^{EV} is the drainage function that takes into account the contribution of the downstream boundary condition for the evapotranspiration fluxes. By applying the same methodology as previously, we deduce the following relationship:

$$D_1^{EV}(L,t)=D_1(L,t)+\Delta_{EV}(L,t), \tag{34}$$

$$\Delta_{EV}(L,t)=max\left(0;(Ev+Tr)\left(1-\frac{L-L_t\tan\psi}{\frac{L_t^2}{2}-\varphi_1}\right)\right). \tag{35}$$

The new drainage function that takes into consideration the evapotranspiration fluxes is linked to the one obtained in the previous section. An additional term just has to be added. We may notice that at $L=0$, i.e., a column located at the river, the drainage function is equal to the evapotranspiration fluxes. In that way, the water table level would remain constant in such a column because the evapotranspiration fluxes are compensated by the drainage function (33). This new term in the drainage formulation must be positive because it represents an inflow of water in the hillslope. When the right hand side of equation (35) becomes negative, it means that the column is too far from the river to be influenced by the boundary condition. There is no coupling between the river and the evapotranspiration. As a consequence, its value must be forced to zero.

Finally, the drainage function, $D(L,t)$, that models the lateral flow through the vertical column in the H2SC model is given by equation (10), where D_1, D_2, f_1, and Δ_{EV} are given by equations (22), (26), (31), and (35), respectively.

2.5. Numerical Implementation

The H2SC model is solved numerically with the Cast3M computer code (website: http://www-cast3m.cea.fr/). This code was developed for solid and fluid mechanics applications at the Commissariat à l'Energie Atomique (CEA, France). It has been used in hydrology and hydrogeology [*Teles et al.*, 2007; *Weill et al.*, 2009; *Mügler et al.*, 2011; *Kollet et al.*, 2017]. The integrated model of surface and subsurface flows is discretized with a finite volume formulation. The equations are solved with an implicit time discretization scheme and an iterative Picard algorithm, except for the drainage function, which is explicitly solved. The time steps automatically adjust between two imposed values to capture short but significant variations in the water flow in the modeled domain and transitions in the saturation of the subsurface.

Atmospheric variables need to be evaluated for the modeling of evapotranspiration fluxes. However, Cast3M is not designed to simulate land-atmosphere interactions. Conversely, Orchidée is a land surface model that was initially developed to couple with atmospheric models and to simulate the climate on a global scale [*Krinner et al.*, 2005]. Evapotranspiration processes are implemented in Orchidée as described in section 2.3. The formulations of the evaporation and transpiration can be decomposed in three main terms: a term depending on the time, another depending on the water content and a final term that represents the vertical distribution of the flux in the soil as follows:

$$tr(z,t)=f_t(t)g_t(\theta(t,z))h_t(z), \tag{36}$$

$$ev(z,t)=\min\left(f_e(t),\ E_p(t)f_{bs}(t)-TR(t)-IN(t)\right)g_e(\theta(t,z))h_e(z)\ , \tag{37}$$

where f_t and f_e are deduced from equations (4) and (6), respectively. These two functions are first evaluated with an Orchidée simulation. Second, a Cast3M simulation is performed imposing tr (equation (36)) and ev (equation (37)) as sink terms in the generalized Richards equation (2). These two functions are calculated

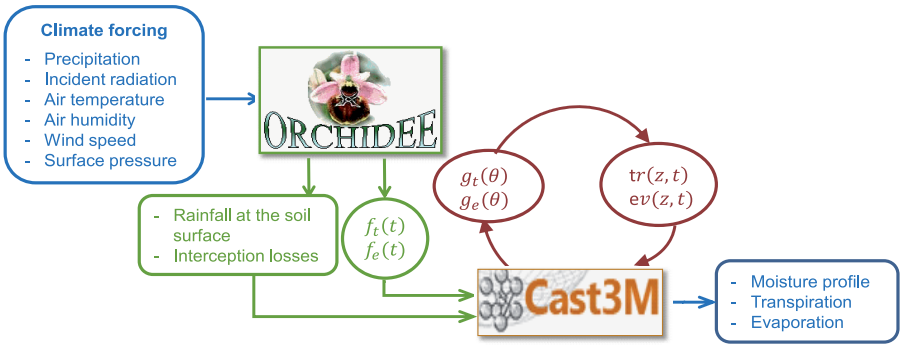

Figure 3. Schematic diagram showing the chaining of Orchidée with Cast3M.

using the values of the soil moisture in the Cast3M simulation and the values of f_t and f_e previously determined from the Orchidée simulation. The functions h_t and h_e are constant over time. This chaining between Orchidée and Cast3M is illustrated in Figure 3. It allows the evapotranspiration fluxes to be more accurately modeled in comparison to an over-simplified parameterization.

The climate forcing for the Orchidée simulations is comprised of seven variables [*Guimberteau et al.*, 2014]. Only the precipitations are reused by the Cast3M simulations. They are imposed as a source term in the generalized Richards equation. The functions f_t (equation (36)) and f_e (equation (37)) deduced from Orchidée simulations are imposed as time series in the Cast3M simulations. Orchidée uses a large number of parameters. Some of them, such as soil parameters, are also used in Cast3M. These common parameters must be consistent between the two codes for a given simulation. The parameters of the drainage function are deduced from the hillslope geometric characteristics.

To limit the impact of the initial conditions in Orchidée, the model is run over several years, and only the final results are used for the chaining. It has been verified that the initial conditions have a negligible impact on the forcing functions (not shown here). Cast3M simulations are initialized with an imposed hydraulic head in the whole column. It corresponds to a given water table level in the column.

3. Numerical Experiments

In this section, we present some of the test cases that have been performed to validate our model approach. For each test case, the time evolution of the water table depth obtained from our column approach (H2SC model) was compared with the results of a complete 2-D simulation performed with Cast3M.

3.1. Description of the Test Cases

The geometry of the configurations is displayed in Figure 1a. The geometric parameters are the same for all four test cases described in this section: $h_r=5$ m, $L_t=50$ m, and $\alpha=\gamma=10\%$. A 2-D simulation representing the entire hillslope was performed for each test case. The results of this simulation were used as a reference. The H2SC model was applied at four various distances from the river: $L=5,\ 15,\ 25,$ and 35 m. The values of all other geometric parameters (h_r, L_t, α, γ, and $x_s(t=0)$) and the values of all soil parameters (K_{sat}, θ_s, θ_r, β, and n) needed for the H2SC model were the same as those used in the 2-D hillslope simulations.

In the first test case, neither the precipitation nor evapotranspiration were imposed. The objective was to validate the D_1 drainage function given by equation (22). Initially, the water table was linear, its slope was equal to 7%, and there was no seepage ($x_s(t=0)=0$). The soil parameters represented a medium-textured soil, and their values were as follows: $K_{sat}=2.89\times10^{-6}$ m/s, $\theta_s=0.43$, $\theta_r=0.078$, $\beta=3.6$ m^{-1}, and $n=1.56$ [*de Rosnay et al.*, 2002]. Fine and coarse-textured soils with different saturated and residual water contents, van Genuchten parameters, and saturated hydraulic conductivities were also tested (results not shown here) [*Maquin*, 2016]. Ninety days were simulated. The second test case implied a rainy period. Its purpose was to involve the D_2 drainage function given in equation (26) and the transition phase between D_1 and D_2. The rainfall rate was 10^{-7} m/s for 5×10^5 s. The initial water table level had a 6% slope. The third test case only involved the evaporation to validate the addition of the Δ_{EV} function given by equation (35). The

evaporative rate was imposed at a constant rate of 10^{-8} m/s over time. In the fourth test case, real forcing data were used. The data were measured at the Amplero tower (Italy) and obtained from the Fluxnet database (http://fluxnet.ornl.gov/site/528). The objective was to test the complete formulation of the drainage function of the H2SC model when the precipitation, evaporation and transpiration varied with time. In this case, the simulation combined the Orchidée model with the Cast3M one to properly simulate the evapotranspiration fluxes from atmospheric data. Orchidée was run using data from 2002 to 2004. The soil was still the medium-textured one, and the vegetation was a grassland (plant functional type number 10 in *Guimberteau* [2010]). For the Cast3M simulations (hillslope and column simulations), only the 2004 results from Orchidée were used. A month without any precipitation or evapotranspiration was added before the 2004 forcing for the hillslope simulation. The aim was to minimize the impact of the initially prescribed water table level on the 2-D results. The initial water level in each column was deduced from the results of the hillslope at the end of the first month of simulation, which represented the beginning of the year 2004 simulation.

3.2. Results and Discussion

The results of the four test cases are displayed in Figure 4. In all cases, the time evolutions of the water table depth obtained from the H2SC model for various distances from the river (dashed lines in Figure 4) are compared with the "reference" results (2-D simulations, solid lines in Figure 4).

Concerning the first test case, we observed a good agreement between the 1-D and 2-D results for the four studied distances (Figure 4a). The RMSE varied between 1 and 5 cm, which is particularly low. The difference between the 1-D and 2-D results slightly increased with the distance from the river. This finding is observed because the water table tends to curve until it is horizontal near the top of the hillslope, where a no flux boundary condition is imposed in the 2-D simulations. As a consequence, the hypothesis of a linear water table in the H2SC model reaches its limit of validity in the upstream part of the hillslope. Some sensitivity studies for various parameters were also performed (not shown here). Only the main conclusions are detailed here. First, the same comparison between the 1-D and the 2-D simulations were performed with two other types of soil: a fine and a coarse-textured soil [*de Rosnay et al.*, 2002]. We obtained the same order

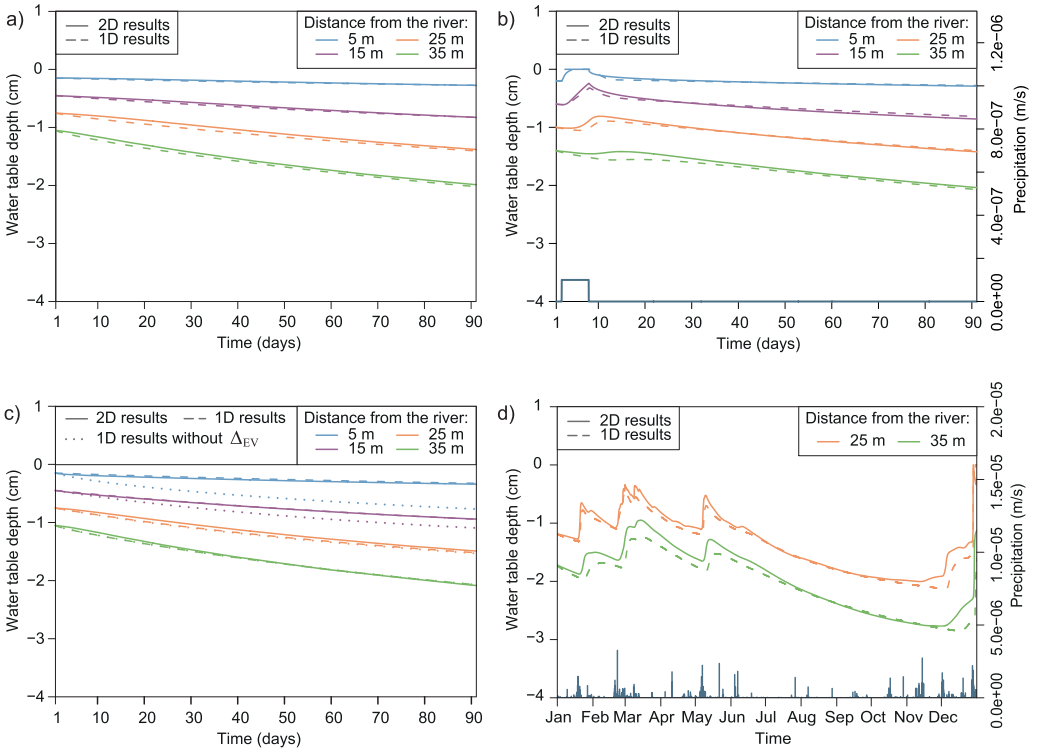

Figure 4. Results of the four test cases: (a) no precipitation, no evapotranspiration, (b) only precipitation, (c) only evaporation, and (d) real forcing from the Orchidée simulation with the Fluxnet database data.

of magnitude for the RMSE regardless of the soil type. We also verified that the initial slope of the water table did not affect the agreement between the 1-D and the 2-D simulations. Concerning the geometric parameters, the slopes α and γ were the main parameters that affected the quality of the results of the H2SC model. The RMSE increased as they increased. The largest errors occurred when the top of the saturated zone was close to the bottom end of the aquifer and hence the bottom of the column, shortly before completely disappearing and leading to an entirely unsaturated column. In this case, the simulated water table elevation in the column decreased to the bottom of the column faster than in the 2-D simulation. This difference is explained by the invalidity of the assumption of a linear water table in this particular case.

The second test case implied a rainfall period. The results are displayed in Figure 4b. The rise of the water table due to the rainfall event was clearly observed, and the 1-D and 2-D time evolutions were in good agreement during this period regardless of the distance of the column from the river. The increase in the water table depth due to infiltration was delayed in the columns compared to the 2-D results, and the maximum value was slightly lower with the 1-D approach. The reason is that the rise in the water table was due to vertical transfers from the unsaturated zone and from lateral diffusion that was not taken into account in the H2SC model. The decrease in the water table level after the rainfall event was well reproduced by the H2SC model. The column located 15 m from the river clearly showed two successive phases during the declining phase: a fast drop just after the rise of the water table and a smoother one later. In the H2SC model, the first phase was related to the D_2 function and the second one to the D_1 function. These two dynamics of dropping were adequately represented by the H2SC model. It should be noted that these observations were confirmed by additional simulations. For higher rates of rainfall, the rise in the water table was more abrupt, such as in the first phase of dropping. In such cases, the differences between the 1-D and 2-D results were higher because the H2SC model failed to reproduce sudden changes. However, after the strong variations, the 1-D simulated water table level converged to the 2-D one, and the agreement was as good as in the first test case without a rainfall event. The time needed to reach the convergence between the 2-D and 1-D results depended on the soil type. The time increased as the soil became finer because the dynamics were slower [*Maquin*, 2016]. Another limitation of the H2SC model occurred when the saturated zone reached the top of the column. In that case, the column was located in the seepage face, and the model could not estimate the length of the seepage face beyond the column. It was assumed that the seepage face did not extend past the column. The distance between the river and the column was then a maximal value for the length of the seepage face. As a consequence, the value of the drainage function may have been inappropriate, and the H2SC model failed to reproduce the decrease of the water table level immediately after the column had been completely saturated.

The purpose of the third case was to validate the modeling of the evaporation in the H2SC model. The results are displayed in Figure 4c. The dashed and dotted lines represent the results of the H2SC model with and without the Δ_{EV} term in the drainage function, respectively. Let us recall here that Δ_{EV} given in equations (34) and (35) is the term in the drainage function that accounts for the influence of the evapotranspiration fluxes on the water table dynamics. As seen in Figure 4c, the temporal evolutions of the water table depth in the columns located at $L=5$ m and at $L=15$ m were significantly improved when the Δ_{EV} term was taken into account. On the contrary, no difference can be observed between the simulations with and without the Δ_{EV} term at $L=25$ m and at $L=35$ m. The two columns were too far from the river. As a consequence, there was no interaction with the boundary condition at the river. Other test cases (not shown here) were performed with other initial water table slopes, rates of evaporation, and vertical distributions of the water uptake. All the cases led us to the same conclusions [*Maquin*, 2016].

The fourth test case involved a real time series of precipitation and evapotranspiration over a whole year. The results are displayed in Figure 4d. Only the two columns located at distances $L=25$ m and $L=35$ m from the river are presented. Indeed, the columns located at $L=5$ m and at $L=15$ m were completely saturated during the rainy period, and the H2SC model was no more appropriate. In this case, a substantial reduction of the calculation time between 2-D and H2SC simulations is observed. The factor of reduction is 15 for $L=25$ m and 20 for $L=35$ m. As shown in Figure 4d, the global trend and the dynamics of the water table level were properly simulated in the two columns. The series of increases and rapid and smooth drops were well captured by the H2SC model. The RMSE was equal to 11 cm and 17 cm at $L=25$ m and $L=35$ m, respectively. The observed discrepancies have already been mentioned in the previous test cases. In particular, we observe a time lapse at the start of the rise of the water table and a lower value of the minimum water depth.

There is no simple analytical expression for giving the critical depth beyond which the water table depth is no more influenced by evapotranspiration. When only evaporation is considered (third case), this depth can be estimated as follows. In this case, evaporation concerns a soil thickness of 20 cm [*Maquin*, 2016] and the β parameter of van Genuchten function is taken equal to 3.6 m^{-1}, which gives a capillary length of 30 cm approximately. This leads to a critical depth that we approximately take equal to 80 cm, i.e., the soil thickness of 20 cm plus two times the capillary length. Therefore, we can estimate that the water table is no more influenced by evaporation when its depth is greater than 80 cm. This is what Figure 4 shows: there is an influence in the columns located at $L=5$ m and at $L=15$ m where the water table depth is smaller than 80 cm although there is no influence for the columns located at $L=25$ m and at $L=35$ m where the depth is greater than 80 cm. When transpiration is taken into account, as in the fourth case, this type of estimation is more difficult to do as the root profile is exponential [*de Rosnay and Polcher*, 1998].

In the four test-cases, the HS2C model showed important reductions of the calculation times in comparison with the hillslope simulations. HS2C simulations of the simplest configuration (first test case), and of the more complicated one (fourth test case) were 3 and 20 times faster, respectively.

4. Application to the Strengbach Catchment

In this section, we present an application of the H2SC model to the Strengbach granitic catchment that is located in the Vosges Mountains (northeastern France). The objective is to test the ability of the column model to simulate the water table variations measured in two piezometers and induced by the 3-D catchment hydrology.

4.1. Site Description

The Strengbach catchment is a small forested watershed that covers an area of 80 ha (Figure 5). The elevation ranges from 883 m above sea level to 1146 m. The climate is temperate oceanic mountainous with a mean annual temperature of +6°C and a monthly average temperature ranging between −2 and +14°C. The mean annual precipitation is approximately 1400 mm, and snowfall occurs from October to April. The

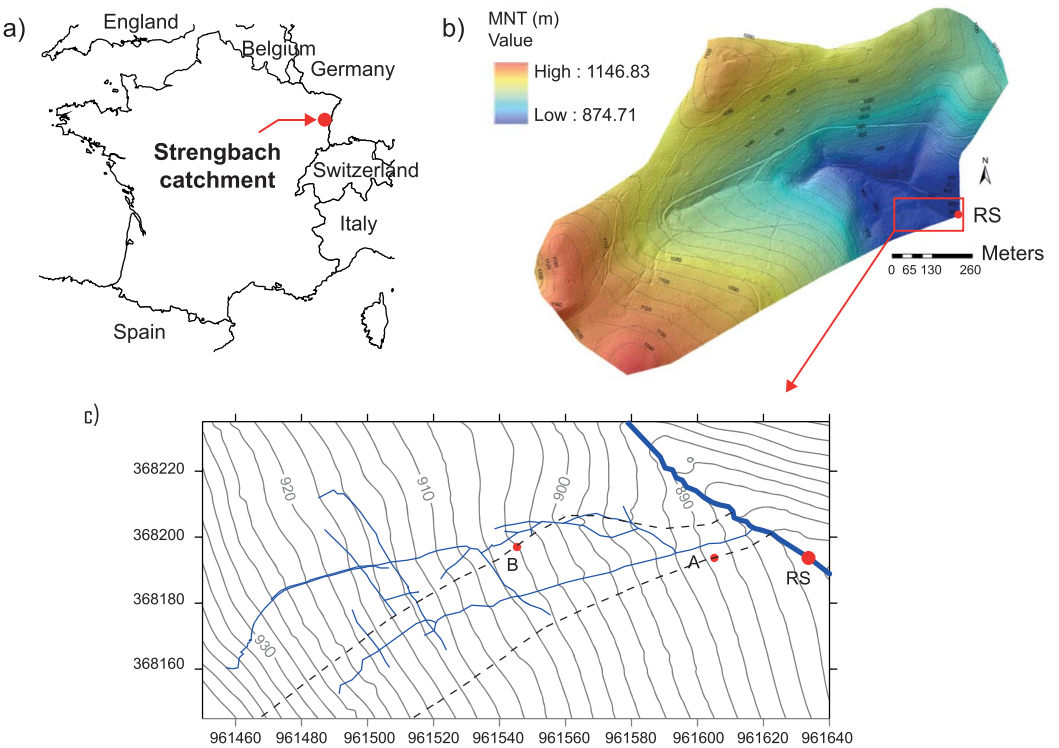

Figure 5. The Strengbach catchment and the position of the piezometers. The hillslope transects that cross piezometers A and B are represented by dashed lines.

mean annual runoff from 1986 to 2006 was 853 mm, and the annual runoff ranged from 525 to 1147 mm [*Pierret et al*., 2014]. Forests cover approximately 90% of the catchment; they are comprised of spruces (80% of the forested area) and beech trees (the remaining 20%). The bedrock is mainly composed of a hydrothermally altered granite on the northern slope [*Ladouche et al*., 2001; *Goddéris et al*., 2006; *Lemarchand et al*., 2012; *Pierret et al*., 2014]. Approximately 10 springs have been identified in the catchment, and some are collected for the water supply [*Pierret et al*., 2014]. The others flow into the stream. A variably saturated area is located near the outlet (Figure 5). Several piezometers have been installed in that zone [*Ladouche et al*., 2001]. The Strengbach catchment has been surveyed since 1986, and meteorological, hydrological, and geochemical data have been recorded. It is now a permanently instrumented environmental observatory (Observatoire Hydro-Géochimique de l'Environnement, OHGE, http://ohge.unistra.fr/). It is worth mentioning the works of *Godderis et al*. [2006] on the use of the soil column model WITCH to study soil and rock weathering processes. Different geochemical studies of the soil and surface waters of the catchment have illustrated the necessity to integrate into soil column models a realistic representation of the hydrological cycle [*Cenki-Toc et al*., 2009; *Godderis et al*, 2009].

4.2. Data and Parameters

Piezometric heads have been measured at an hourly time step during several months in only two piezometers, denoted A and B in Figure 5. Hence, we selected these two piezometers for modeling with the H2SC model. Temporal evolutions of the water table depth in A and B were compared with simulated ones. Piezometers A and B are located in a spruce area and in a clearing, respectively. The soil and vegetation parameters required for the model were obtained from *Biron* [1994]. The soil parameters (K_{sat}, θ_s, θ_r, β, and n) correspond to data obtained from samples extracted from an old area of spruces in the catchment, such as the area where piezometer A is located. The same values were used for the modeling of piezometer B because no specific study has been conducted for the clearing. The distribution with depth of the soil properties was characterized between the surface and a depth of 1 m. Below a depth of 1 m, the values were constant.

The root profile for the spruce species was deduced from field observations ($h_t(z)$ in equation (36)). Three depth ranges were isolated and assigned root density values: 30% of the roots were located in the top 10 cm, 60% were between depths of 10 and 70 cm, and the remaining 10% were between depths 70 cm and 1 m. Concerning the clearing, the root profile followed an exponential function as in *de Rosnay and Polcher* [1998] that had an exponential coefficient of 4 and a maximum depth of 2 m. This finding corresponded to the representation of grassland in Orchidée [*Guimberteau*, 2010]. Soil macroporosity due to the roots was observed in the field [*Biron*, 1994]. To model the rapid flow through the macropores, the hydraulic conductivity K_{sat} was set to 10^{-3} m/s in the first 60 cm of the soil for the spruces and in the first 40 cm for the clearing [*Shi et al*., 2013; *Milly et al*., 2014].

The ranges in the geometric parameters for the H2SC model (L, L_t, h_r, α, and γ in Figure 1a) were inferred from a consideration of the location of the piezometers in the catchment and from expert knowledge. In the H2SC model, each of the two columns corresponding to the piezometers' locations must be associated with a hillslope. Those hillslopes were defined along the steepest surface slope from the watershed divide to the river intersecting the location of the piezometers. They were deduced from topographic information. The distances of piezometers A and B from the river were approximately 20 m and 70 m, respectively. The total length of the hillslope (L_t in Figure 1a) was evaluated at approximately 200 m and 600 m, respectively. The surface slope (γ in Figure 1a) was approximately 26% for both cases. The aquifer height below the river (h_r in Figure 1a) was estimated to be between 2 and 3 m, with a slight increase along the hillslope from the stream to the hilltop. No data were available for the aquifer slope that was estimated to 10% (α in Figure 1a).

The forcing data imposed on the Orchidée simulations originated from two sources. Rainfall, air temperature and wind data have been measured in the Strengbach catchment. Because some parameters are unavailable, including humidity, surface shortwave and longwave radiation and surface pressure, outputs of the meteorological analysis model SAFRAN were used [*Durand et al*., 1993, 2009; *Quintana-Seguí et al*., 2008; *Vidal et al*., 2010]. Forcing data needed for the Cast3M simulations were then extracted from the results of the Orchidée simulation. Two periods of forcing data were obtained by merging the local measurements and SAFRAN data set. The first one began on 11 April 1996, and ended at the end of the day on 23 July

1996. The second period was from 13 April 1997, to 13 October 1997. The periods corresponded to the measurement periods of piezometers A and B at an hourly time step.

Initially, a constant head was prescribed in the H2SC columns. The value of the water table depth was measured in the corresponding piezometer at the beginning of the period. However, two model parameters had to be initialized: the slope of the linear water table $i(t=0)$ and the length of the seepage face $x_s(t=0)$. They were linked to the initial water table depth, but they could not be differentiated from this unique data.

4.3. Calibration and Validation Simulations

Because of the lack of measurements and lack of confidence in the geometric and physical parameters, some model parameters were subjected to a calibration procedure. The HydroPSOR package was used, which performs sensitivity analyses and model calibrations. Several studies have shown that the HydroPSO R package is efficient for calibration [*Zambrano-Bigiarini and Rojas*, 2013; *Abdelaziz and Zambrano-Bigiarini*, 2014; *Brauer et al*., 2014b].

First, a sensitivity analysis was performed for piezometer A in the first data period (11 April 1996 to 23 July 1996). Thirteen relevant model parameters were selected (geometric and physical parameters). Their respective ranges originated from the ranges of the parameters in *Biron* [1994], from a spatial analysis of the catchment, expert knowledge of the catchment (cf. section 4.2), and the first calibration attempts. The performance of each simulation was assessed using the root-mean-square error (RMSE) indicator applied to the water table depth results. The sensitivity analysis showed that the model was particularly sensitive to five parameters [*Maquin*, 2016]. Two of the five sensitive parameters characterized the soil (the van Genuchten parameter n and the saturated hydraulic conductivity of the lower soil layer K_{sat}). The remaining three parameters characterized the geometry (the surface slope, γ, the length of the hillslope, L_t, and the aquifer height below the river, h_r). The five parameters were selected for the calibration procedure of the piezometer A.

The RMSE was used as the goodness of fit measure for the calibration. The investigated ranges for the parameters were the same as those investigated in the sensitivity analysis. The optimal set of parameters implied an RMSE of 0.066 m. The corresponding evolution of the water table depth over time is displayed in Figure 6a.

The calibrated parameters were then used to simulate the second period of data (13 April 1997 to 13 October 1997) for piezometer A. The objective was to test whether the values obtained from the calibration procedure were still valid for another forcing data signal. The values of the parameters were the same as for the calibration study, except for the initial water table depth and the initial length of the seepage face that were set to 0.68 m and 0 m, respectively, to match the measured water table depth on 13 April 1997. The results for this simulation are shown in Figure 6b.

The water table depth in piezometer B was also simulated for the two periods. The soil parameter values were kept the same as those used for the piezometer A simulations. However, the vegetation and geometric parameters were different. The length of the initial seepage face was set to 2 m, which was taken from a manual calibration. The initial water table depth was set to 0.27 m. The simulation of the second period should have differed from the simulation of the first period only due to the initialization. Fortuitously, the initial water table depth was the same for the two periods, and the initial length of the seepage face was set to 0 m.

4.4. Discussion

Regarding the calibrated results of piezometer A, we observed that the simulated water table depth obtained using the H2SC model was in good agreement with the corresponding observations (cf. Figure 6a). This observation was supported by both a relatively high value of the coefficient of determination ($R^2 = 0.68$) and a low RMSE. The general trend of the water table depth was well reproduced by the H2SC model, with several alternations of rising and dropping phases due to the succession of rainy periods. However, there were some discrepancies during particular dropping phases. They essentially occurred in the second part of the simulation when the evaporative demand became more important at the beginning of the summer period. Those discrepancies may not have arisen only from the discharge function proposed in the H2SC model. They may also be explained by an inadequate parametrization or an ill calibration of the

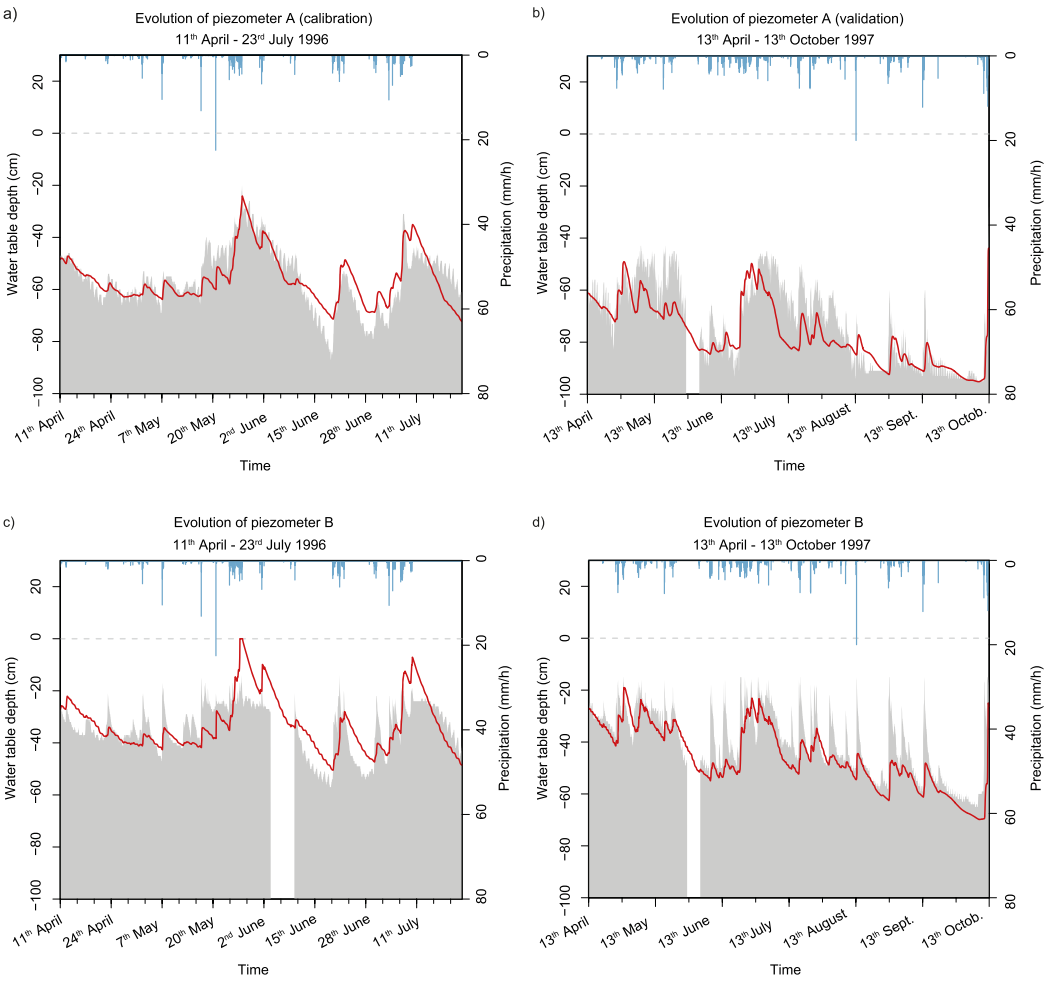

Figure 6. Evolution of the water table depth over time: (a) best-fit simulation (in red) of the calibration study for piezometer A, period 1, (b) simulation of piezometer A, period 2, (c) simulation of piezometer B, period 1, and (d) simulation of piezometer B, period 2. The shaded gray zones represent the measured water levels.

evapotranspiration model of Orchidée. Another difference was also observed; the daily variability in the water table level was not captured by the H2SC model. This variability can be explained by the diurnal cycle of the evaporative demand [*White*, 1932; *Loheide*, 2008; *Miller et al*., 2010;*Grimaldi et al*., 2015]. Once again, those differences can be mainly explained by the evapotranspiration part of the model. As a consequence, the discharge function developed in the present paper seems to properly model the temporal evolution of the water table level.

The second run for piezometer A was applied to the second period of data with the calibrated parameters (cf. Figure 6b). As was the case during the calibrated period, the global trend in the water table level was well reproduced (R^2=0.70 and *RMSE*=0.10 m). It globally decreased until the end of the summer period and alternatively rose and fell in phases that perfectly corresponded to the rainy periods. However, the simulated water level sometimes began to decrease too early compared to the measurements. It seems that there would be a lack of water supply in the model during this period. One reason can be advanced; the runoff may have occurred upstream of the piezometer due to local topographic variations, leading to a longer infiltration period after a rainfall. However, despite those discrepancies, the general trend was not affected, and the lowest water table level at the end of the summer was accurately simulated with the H2SC model.

The results for piezometer B are shown in Figures 6c and 6d for periods 1 and 2, respectively. In both cases, the RMSE and R^2 indicators suggest the fairly good quality of the simulations (R^2=0.43 and 0.66, and *RMSE* =0.08 m and 0.10 m, respectively). Looking in further detail, we observed that the peak values of the

increases in the water table level were not reproduced by the H2SC model. In general, the levels before and after rainfall events were well simulated, but the modeled levels did not increase enough. This observation was previously noted in the test cases section (section 3.2), emphasizing that these differences are directly consequences of the H2SC model. Nevertheless, despite temporary underestimations, the general evolution of the water table level was not impacted. As for piezometer A during period 1, we observe that the drop was too slow during June after the two rainy periods. It strengthened the hypothesis that the gaps were mostly due to errors in the evapotranspiration estimations. Finally, the maximum measured water level seemed to be limited to approximately a depth of 20 cm, whereas the simulation results were higher than that value. Because piezometer B is located on a small and local soil elevation and due to the macropore network near the surface, the water can flow rapidly downstream of the 20 cm soil surface layer. This may explain the limit in the measurement of the water level and the differences with the simulated one. Finally, if we do not take into account the occasional differences just underlined, the H2SC model appeared to be able to simulate the main evolution of the water table level over time.

These calibration results show that the 1-D soil column model H2SC can simulate the water table variations measured in the two piezometers A and B and induced by the 3-D catchment hydrology. This means that the linear water table and the 2-D plan hillslope approximations hold at these two locations. Nevertheless, one must have in mind that the model may have not captured all the hydrological processes taking place in the well area and may have been therefore "over-calibrated" to compensate these non represented processes [*Beven*, 2005; *Gupta et al*., 2012]. As discussed in section 2.4, the linear water table assumption is justified for gentle and uniform slopes, and for shallow and permeable soils. It is known that soils in the mountainous catchments of Vosges Mountains have these properties [*Biron*, 1994]. Figure 5 shows that the hillslope at piezometers A and B is approximately uniform and the slope also, except near the catchment south boundary where the soil slope is twice as large as the slope in the piezometers area. If we consider another area of the Strengbach where the groundwater flow is convergent, at the head of the catchment for instance, or divergent, it is clear that the assumptions of the model do not hold anymore [*Troch et al*., 2003]. Nevertheless, one could apply the HS2C model with the mean slope value as a first approximation if both the cross section of the stream tube that defines the 3-D hillslope, denoted hillslope width function by *Troch et al*. [2003], and the soil slope do not "vary much" along the hillslope longitudinal axis. However, there is no rule setting the validity limits of such an extension to 3-D hydrologic contexts and these limits have to be defined and tested for each catchment.

5. Conclusions

A new hydrological hillslope-based soil column model, which is denoted H2SC, that realistically represents water table dynamics has been presented. It is based on a novel approach for incorporating the total lateral fluxes in a column model. Instead of solving the 2-D generalized Richards equation at the hillslope scale, the lateral fluxes through a given soil column along the hillslope are estimated. This estimation is then imposed as a source/sink term at the bottom of the column, which is called the drainage function. The introduced drainage function leads to a realistic simulation of the temporal evolution of the water table depth in a soil column that belongs to a specific hillslope. The evaluation of this function is based on physically based equations of the hydrological behavior at the hillslope scale and on simplifying assumptions such as a linear water table along a hillslope with a varying seepage face. The level of simplification is coherent with the physics that is usually introduced in soil column models considering that they may be used for computer time demanding simulations. The drainage function accounts for the geometry of the steepest slope of the catchment that intersects the location of the column, and for soil and vegetation parameters. As a consequence, it is not a site-specific equation. Different hydrological regimes leading to different formulations of the drainage function were distinguished (no seepage face case, seepage face case with a nearby column, and seepage face case with a distant column). The drainage function finally depends on two newly introduced and time-varying variables: the angle of the linear water table level and the length of the seepage face. These two variables are updated at each time step according to the hydrological regime. The impact of the evapotranspiration fluxes on the water table level has also been included in the drainage function. Finally, this column model simulates the temporal evolution of the water table depth and of the evapotranspiration fluxes while taking into account their interaction. For a given hillslope, the model is able to represent the impact of a near-surface water table on evapotranspiration fluxes. For instance, columns

located near the river have a higher water table and consequently higher evapotranspiration fluxes. These mathematical developments may seem complex, but the drainage function is finally relatively simple. Its implementation does not raise any difficulties and its numerical resolution is straightforward.

The H2SC model was first validated using numerical experiments. Column simulations were compared to 2-D reference simulations of a hillslope. Distances along the hillslope were selected to compare the 1-D and the 2-D simulations. Different climate forcings, soil types, and geometric parameters were tested. In the second part, the H2SC model was applied to the locations of two piezometers in the Strengbach catchment, France, during two periods. The parameters of the H2SC model were calibrated using the first piezometer during the first period. The calibrated parameters were then applied to the second period and to the second piezometer in the two periods. Globally, considering all the tested cases, the H2SC model was able to model the rising and dropping phases of the water table due to rainy events at a daily scale and also the general trend at a seasonal scale. The application to a 3-D hydrologic situation showed also that the use of the column model to simulate locally the water table in a catchment is possible and makes sense, provided a number of conditions on the local catchment characteristics are met.

The ability of HS2C to simulate the piezometry of a catchment is one of the perspectives of the model. The comparison between the hydraulic head distributions simulated with a 3-D hydrologic code and with HS2C at different points in a catchment would allow to set the limits of validity of the soil column model approach, both inside a catchment and for different types of catchment. Moreover, it would also allow to address different issues raised by the assumptions of the model such as: how to take into account the land cover spatial variability, the soil heterogeneity or a nonuniform rainfall rate distribution?

Appendix A

The potential evapotranspiration (E_p in equation (4)) is proportional to the gradient of specific humidity between air (q_a) and air at saturation for soil temperature ($q_s(T_s)$):

$$E_p(t)=\frac{\rho}{r_a}(q_s(T_s)-q_a), \tag{A1}$$

where ρ is the air density and r_a is the aerodynamic resistance. The bare soil fraction (f_{bs} in equation (4)) is computed as follows:

$$f_{bs}(t)=e^{-c\times LAI}, \tag{A2}$$

where c is an extinction coefficient depending on the type of vegetation and LAI is the leaf area index [*d'Orgeval*, 2006].

The resistance function (f_{r1} in equation (4)) is expressed as:

$$f_{r1}(t)=\frac{1}{1+\frac{r_c+r_0}{r_a}}, \tag{A3}$$

where r_c is the canopy resistance, r_0 is the architectural resistance. More details about these variables can be found in *de Rosnay and Polcher* [1998].

The water availability function ($g_t(\theta)$ in equation (4)) is a function of nodal water content. It represents the ability of roots to extract water depending on water content. The shape of this function is similar to the one used in Orchidée [*de Rosnay et al.*, 2002]. It depends on two parameters, θ_w and θ_d. θ_w is the wilting point, i.e., the water content below which the roots are not able to extract water anymore. θ_d is the water content above which the root water uptake is maximal.

The water availability function for evaporation ($g_e(\theta)$ in equation (6)) is similar to the one for transpiration. The difference is that the two characteristic water content variables (θ_w and θ_d) are replaced by two other values, θ_1 and θ_2, respectively. θ_1 is the moisture content below which evaporation is zero and θ_2 is the moisture content above which full evaporation can occur.

Similarly to the evapotranspiration fluxes, the interception losses ($IN(t)$ in equation (6)) depend on potential evapotranspiration and they take into account the leaves' exposure to the air. Moreover, the amount of water available on the foliage limits this flux.

$$IN(t) = \min\left(I, E_p \frac{I}{I_{max}} f_{r2}\right), \tag{A4}$$

where f_{r2} is a resistance function expressed as follows:

$$f_{r2}(t) = \frac{1}{1 + \frac{r_0}{r_a}}. \tag{A5}$$

Acknowledgments
The authors would like to thank Agnès Ducharne (UMR METIS, CNRS/UPMC, France) for supporting this work. This work has been funded by the LEFE program of the French National Center for Scientific Research (CNRS/INSU). The authors are thankful to three anonymous reviewers for their suggestions and constructive comments. The data used in the study can be obtained from the corresponding author.

References

Abdelaziz, R., and M. Zambrano-Bigiarini (2014), Particle Swarm Optimization for inverse modeling of solute transport in fractured gneiss aquifer, *J. Contam. Hydrol.*, *164*, 285–298, doi:10.1016/j.jconhyd.2014.06.003.

Anyah, R. O., C. P. Weaver, G. Miguez-Macho, Y. Fan, and A. Robock (2008), Incorporating water table dynamics in climate modeling: 3. Simulated groundwater influence on coupled land-atmosphere variability, *J. Geophys. Res.*, *113*, D07103, doi:10.1029/2007JD009087.

Bear, J. (1972), *Dynamics of Fluids in Porous Media*, Am. Elsevier Publ. Co., New York.

Beven, K. J. (2005), On the concept of model structural error, *Water Sci. Technol.*, *52*(6), 167–175.

Beven, K. J., and M. J. Kirkby (1979), A physically based, variable contributing area model of basin hydrology, *Hydrol. Sci. B.*, *24*(1), 43–69, doi:10.1080/02626667909491834.

Biron, P. (1994), Le cycle de l'eau en forêt de moyenne montagne: Flux de sêve et bilans hydriques stationnels, Thèse de doctorat, Univ. Louis Pasteur, Strasbourg.

Brauer, C. C., A. J. Teuling, P. J. J. F. Torfs, and R. Uijlenhoet (2014a), The Wageningen Lowland Runoff Simulator (WALRUS): A lumped rainfall-runoff model for catchments with shallow groundwater, *Geosci. Model Dev.*, *7*(5), 2313–2332, doi:10.5194/gmd-7-2313-2014.

Brauer, C. C., P. J. J. F. Torfs, A. J. Teuling, and R. Uijlenhoet (2014b), The Wageningen Lowland Runoff Simulator (WALRUS): Application to the Hupsel Brook catchment and the Cabauw polder, *Hydrol. Earth Syst. Sci.*, *18*(10), 4007–4028, doi:10.5194/hess-18-4007-2014.

Campoy, A., A. Ducharne, F. Cheruy, F. Hourdin, J. Polcher, and J. C. Dupont (2013), Response of land surface fluxes and precipitation to different soil bottom hydrological conditions in a general circulation model, *J. Geophys. Res. Atmos.*, *118*, 10,725–10,739, doi:10.1002/jgrd.50627.

Carrillo, G., P. A. Troch, M. Sivapalan, T. Wagener, C. Harman, and K. Sawicz (2011), Catchment classification: Hydrological analysis of catchment behavior through process-based modeling along a climate gradient, *Hydrol. Earth Syst. Sci.*, *15*(11), 3411–3430, doi:10.5194/hess-15-3411-2011.

Cenki-Tok, B., F. Chabaux, D. Lemarchand, A. D. Schmitt, M. C. Pierret, D. Viville, and P. Stille (2009), The impact of water-rock interaction and vegetation on calcium isotope fractionation in soil-and stream waters of a small, forested catchment (the Strengbach case), *Geochim. Cosmochim. Acta.*, *73*(8), 2215–2228.

Chen, L., L. Wang, Y. Ma, and P. Liu (2015), Overview of ecohydrological models and systems at the watershed scale, *IEEE Syst. J.*, *9*(3), 1091–1099, doi:10.1109/JSYST.2013.2296979.

Condon, L. E., R. M. Maxwell, and S. Gangopadhyay (2013), The impact of subsurface conceptualization on land energy fluxes, *Adv. Water Resour.*, *60*, 188–203, doi:10.1016/j.advwatres.2013.08.001.

Coon, E. T., J. D. Moulton, and S. L. Painter (2016), Managing complexity in simulations of land surface and near-surface processes, *Environ. Modell. Software*, *78*, 134–149, doi:10.1016/j.envsoft.2015.12.017.

Dai, Y. J., et al. (2003), The common land model, *Bull. Am. Meteorol. Soc.*, *84*(8), 1013–1023, doi:10.1175/BAMS-84-8-1013.

Decharme, B., A. Boone, C. Delire, and J. Noilhan (2011), Local evaluation of the Interaction between Soil Biosphere Atmosphere soil multilayer diffusion scheme using four pedotransfer functions, *J. Geophys. Res.*, *116*, D20126, doi:10.1029/2011JD016002.

Durand, Y., E. Brun, L. Merindol, G. Guyomarch, B. Lesaffre, and E. Martin (1993), A meteorological estimation of relevant parameters for snow models, in *Proceedings of the Symposium on Snow and Snow-Related Problems*, *Ann. Glaciol.*, edited by S. C. Colbeck, vol. 18, pp. 65–71, Int. Glaciol. Soc., Cambridge, U. K.

Durand, Y., G. Giraud, M. Laternser, P. Etchevers, L. Merindol, and B. Lesaffre (2009), Reanalysis of 47 years of climate in the French Alps (1958–2005): Climatology and trends for snow cover, *J. Appl. Meteorol. Climatol.*, *48*(12), 2487–2512, doi:10.1175/2009JAMC1810.1.

Fan, Y., and R. L. Bras (1998), Analytical solutions to hillslope subsurface storm flow and saturation overland flow, *Water Resour. Res.*, *34*(4), 921–927, doi:10.1029/97WR03516.

Fan, Y., H. Li, and G. Miguez-Macho (2013), Global patterns of groundwater table depth, *Science*, *339*(6122), 940–943, doi:10.1126/science.1229881.

Feddes, R. A., et al. (2001), Modeling root water uptake in hydrological and climate models, *Bull. Am. Meteorol. Soc.*, *82*(12), 2797–2809.

Fernandez-Illescas, C. P., and I. Rodriguez-Iturbe (2003), Hydrologically driven hierarchical competition-colonization models: The impact of interannual climate fluctuations, *Ecol. Monogr.*, *73*(2), 207–222.

Ford, T. W., A. D. Rapp, S. M. Quiring, and J. Blake (2015), Soil moisture–precipitation coupling: Observations from the Oklahoma Mesonet and underlying physical mechanisms, *Hydrol. Earth Syst. Sci.*, *19*(8), 3617–3631, doi:10.5194/hess-19-3617-2015.

d'Orgeval, T. (2006), Impact du changement climatique sur le cycle de l'eau en Afrique de l'Ouest: Modélisation et incertitudes, Thèse de doctorat, Univ. Pierre et Marie Curie, Paris.

de Rosnay, P. (1999), Représentation de l'interaction sol-végétation-atmosphère dans le modèle de circulation générale du Laboratoire de Météorologie Dynamique, Thèse de doctorat, Univ. Pierre et Marie Curie, Paris.

de Rosnay, P., and J. Polcher (1998), Modelling root water uptake in a complex land surface scheme coupled to a GCM, *Hydrol. Earth Syst. Sci.*, *2*(2–3), 239–255, doi:10.5194/hess-2-239-1998.

de Rosnay, P., J. Polcher, M. Bruen, and K. Laval (2002), Impact of a physically based soil water flow and soil-plant interaction representation for modeling large-scale land surface processes, *J. Geophys. Res.*, *107*(D11), ACL 3–1–ACL 3–19, doi:10.1029/2001JD000634.

Goddéris, Y., L. M. François, A. Probst, J. Schott, D. Moncoulon, D. Labat, and D. Viville (2006), Modelling weathering processes at the catchment scale: The WITCH numerical model, *Geochim. Cosmochim. Acta*, *70*(5), 1128–1147, doi:10.1016/j.gca.2005.11.018.

Goddéris, Y., C. Roelandt, J. Schott, M. C. Pierret, and L. M. François (2009), Towards an integrated model of weathering, climate, and biospheric processes, *Rev. Mineral. Geochem.*, *70*(1), 411–434.

Graham, D. N., and M. B. Butts (2005), Flexible, integrated watershed modelling with MIKE SHE, in *Watershed Models*, edited by V. P. Singh and D. K. Frevert, pp. 245–272, Taylor and Francis, Boca Raton, Fla.

Grimaldi, S., F. Orellana, and E. Daly (2015), Modelling the effects of soil type and root distribution on shallow groundwater resources, *Hydrol. Processes*, *29*(20), 4457–4469, doi:10.1002/hyp.10503.

Guimberteau, M. (2010), Modélisation de l'hydrologie continentale et influences de l'irrigation sur le cycle de l'eau, Thèse de doctorat, Univ. Pierre et Marie Curie, Paris.
Guimberteau, M., A. Ducharne, P. Ciais, J. P. Boisier, S. Peng, M. De Weirdt, and H. Verbeeck (2014), Testing conceptual and physically based soil hydrology schemes against observations for the Amazon Basin, *Geosci. Model Dev.*, *7*(3), 1115–1136, doi:10.5194/gmd-7-1115-2014.
Gupta, H. V., M. P. Clark, J. A. Vrugt, G. Abramowitz, and M. Ye (2012), Towards a comprehensive assessment of model structural adequacy, *Water Resour. Res.*, *48*, W08301, doi:10.1029/2011WR011044..
Habets, F., et al. (2008), The SAFRAN-ISBA-MODCOU hydrometeorological model applied over France, *J. Geophys. Res.*, *113*, D06113, doi:10.1029/2007JD008548.
Hazenberg, P., Y. Fang, P. Broxton, D. Gochis, G.-Y. Niu, J. D. Pelletier, P. A. Troch, and X. Zeng (2015), A hybrid-3D hillslope hydrological model for use in Earth system models, *Water Resour. Res.*, *51*, 8218–8239, doi:10.1002/2014WR016842.
Hazenberg, P., P. Broxton, D. Gochis, G.-Y. Niu, L. A. Pangle, J. D. Pelletier, P. A. Troch, and X. Zeng (2016), Testing the hybrid-3-D hillslope hydrological model in a controlled environment, *Water Resour. Res.*, *52*, 1089–1107, doi:10.1002/2015WR018106.
Jiang, X., G.-Y. Niu, and Z.-L. Yang (2009), Impacts of vegetation and groundwater dynamics on warm season precipitation over the Central United States, *J. Geophys. Res.*, *114*, D06109, doi:10.1029/2008JD010756.
Kollet, S. J., and R. M. Maxwell (2008), Capturing the influence of groundwater dynamics on land surface processes using an integrated, distributed watershed model, *Water Resour. Res.*, *44*, W02402, doi:10.1029/2007WR006004.
Kollet, S., et al. (2017), The integrated hydrologic model intercomparison project, IH-MIP2: A second set of benchmark results to diagnose integrated hydrology and feedbacks, *Water Resour. Res.*, *53*, 867–890, doi:10.1002/2016WR019191.
Krinner, G., N. Viovy, N. de Noblet-Ducoudré, J. Ogée, J. Polcher, P. Friedlingstein, P. Ciais, S. Sitch, and I. C. Prentice (2005), A dynamic global vegetation model for studies of the coupled atmosphere-biosphere system, *Global Biogeochem. Cycle*, *19*, GB1015, doi:10.1029/2003GB002199.
Ladouche, B., A. Probst, D. Viville, S. Idir, D. Baqué, M. Loubet, J.-L. Probst, and T. Bariac (2001), Hydrograph separation using isotopic, chemical and hydrological approaches (Strengbach catchment, France), *J. Hydrol.*, *242*(3–4), 255–274, doi:10.1016/S0022-1694(00)00391-7.
Lemarchand, D., D. Cividini, M.-P. Turpault, and F. Chabaux (2012), Boron isotopes in different grain size fractions: Exploring past and present water-rock interactions from two soil profiles (Strengbach, Vosges Mountains), *Geochim. Cosmochim. Acta*, *98*, 78–93, doi:10.1016/j.gca.2012.09.009.
Leung, L. R., M. Huang, Y. Qian, and X. Liang (2011), Climate-soil-vegetation control on groundwater table dynamics and its feedbacks in a climate model, *Clim. Dyn.*, *36*(1–2), 57–81, doi:10.1007/s00382-010-0746-x.
Li, Q., A. J. A. Unger, E. A. Sudicky, D. Kassenaar, E. J. Wexler, and S. Shikaze (2008), Simulating the multi-seasonal response of a large-scale watershed with a 3D physically-based hydrologic model, *J. Hydrol.*, *357*(3–4), 317–336, doi:10.1016/j.jhydrol.2008.05.024.
Liang, X., D. Lettenmaier, E. Wood, and S. Burges (1994), A Simple Hydrologically Based Model of Land-Surface Water and Energy Fluxes for General-Circulation Models, *J. Geophys. Res.*, *99*(D7), 14,415–14,428, doi:10.1029/94JD00483.
Liu, D., F. Tian, H. Hu, M. Lin, and Z. Cong (2012), Ecohydrological evolution model on riparian vegetation in hyperarid regions and its validation in the lower reach of Tarim River, *Hydrol. Processes*, *26*(13), 2049–2060, doi:10.1002/hyp.8313.
Loheide, S. P., II (2008), A method for estimating subdaily evapotranspiration of shallow groundwater using diurnal water table fluctuations, *Ecohydrol.*, *1*(1), 59–66, doi:10.1002/eco.7.
Mahrt, L., and H. Pan (1984), A two-layer model of soil hydrology, *Boundary Layer Meteorol.*, *29*(1), 1–20, doi:10.1007/BF00119116.
Maquin, M. (2016), Développement d'un modèle hydrologique de colonne représentant l'interaction nappe-végétation-atmosphère et applications à l'échelle du bassin versant. Thèse de doctorat, Univ. Paris-Saclay, Paris.
Maxwell, R. M., and N. L. Miller (2005), Development of a coupled land surface and groundwater model, *J. Hydrometeorol.*, *6*(3), 233–247, doi:10.1175/JHM422.1.
Maxwell, R. M., and S. J. Kollet (2008), Interdependence of groundwater dynamics and land-energy feedbacks under climate change, *Nat. Geosci.*, *1*(10), 665–669, doi:10.1038/ngeo315.
Miguez-Macho, G., and Y. Fan (2012), The role of groundwater in the Amazon water cycle: 2. Influence on seasonal soil moisture and evapotranspiration, *J. Geophys. Res.*, *117*, D15114, doi:10.1029/2012JD017540.
Miller, G. R., X. Chen, Y. Rubin, S. Ma, and D. D. Baldocchi (2010), Groundwater uptake by woody vegetation in a semiarid oak Savanna, *Water Resour. Res.*, *46*, W10503, doi:10.1029/2009WR008902.
Milly, P. C. D., S. L. Malyshev, E. Shevliakova, K. A. Dunne, K. L. Findell, T. Gleeson, Z. Liang, P. Phillips, R. J. Stouffer, and S. Swenson (2014), An enhanced model of land water and energy for global hydrologic and earth-system studies, *J. Hydrometeorol.*, *15*(5), 1739–1761, doi:10.1175/JHM-D-13-0162.1.
Mügler, C., O. Planchon, J. Patin, S. Weill, N. Silvera, P. Richard, and E. Mouche (2011), Comparison of roughness models to simulate overland flow and tracer transport experiments under simulated rainfall at plot scale, *J. Hydrol.*, *402*(1–2), 25–40, doi:10.1016/j.jhydrol.2011.02.032.
Niswonger, R. G., D. E. Prudic, and R. S. Regan (2006), Documentation of the Unsaturated-Zone Flow (UZF1) Package for modeling unsaturated flow between the land surface and the water table with MODFLOW-2005, *U.S. Geol. Surv. Tech. and Methods 6-A19*, 62 pp.
Niu, G.-Y., et al. (2011), The community Noah land surface model with multiparameterization options (Noah-MP): 1. Model description and evaluation with local-scale measurements, *J. Geophys. Res.*, *116*, D12109, doi:10.1029/2010JD015139.
Ogden, F. L., and B. A. Watts (2000), Saturated area formation on nonconvergent hillslope topography with shallow soils: A numerical investigation, *Water Resour. Res.*, *36*(7), 1795–1804, doi:10.1029/2000WR900091.
Pierret, M. C., P. Stille, J. Prunier, D. Viville, and F. Chabaux (2014), Chemical and U-Sr isotopic variations in stream and source waters of the Strengbach watershed (Vosges mountains, France), *Hydrol. Earth Syst. Sci.*, *18*(10), 3969–3985, doi:10.5194/hess-18-3969-2014.
Quintana-Seguí, P., P. Le Moigne, Y. Durand, E. Martin, F. Habets, M. Baillon, C. Canellas, L. Franchisteguy, and S. Morel (2008), Analysis of near-surface atmospheric variables: Validation of the SAFRAN analysis over France, *J. Appl. Meteorol. Climatol.*, *47*(1), 92–107, doi:10.1175/2007JAMC1636.1.
Ridolfi, L., P. D'Odorico, and F. Laio (2006), Effect of vegetation-water table feedbacks on the stability and resilience of plant ecosystems, *Water Resour. Res.*, *42*, W01201, doi:10.1029/2005WR004444.
Rodriguez-Iturbe, I., A. Porporato, F. Laio, and L. Ridolfi (2001), Plants in water-controlled ecosystems: Active role in hydrologic processes and response to water stress: I. Scope and general outline, *Adv. Water Res.*, *24*(7), 695–705, doi:10.1016/S0309-1708(01)00004-5.
Shi, Y., K. J. Davis, C. J. Duffy, and X. Yu (2013), Development of a coupled land surface hydrologic model and evaluation at a critical zone observatory, *J. Hydrometeorol.*, *14*(5), 1401–1420, doi:10.1175/JHM-D-12-0145.1.
Teles, V., P. Maugis, E. Mouche, J. Brulhet, J. Wendling, and G. Vigneron (2007), Impact of the landscape evolution on the hydraulic boundary conditions of the Callovo-Oxfordian formation, *Phys. Chem. Earth, Parts A/B/C*, *32*(1–7), 359–367, doi:10.1016/j.pce.2005.10.005.

Troch, P. A., C. Paniconi, and E. Emiel van Loon (2003), Hillslope-storage Boussinesq model for subsurface flow and variable source areas along complex hillslopes: 1. Formulation and characteristic response, *Water Resour. Res.*, *39*(11), 1316, doi:10.1029/2002WR001728.

Twarakavi, N. K. C., J. Šimůnek, and S. Sophia (2008), Evaluating interactions between groundwater and vadose zone using the HYDRUS-based flow package for MODFLOW, *Vadose Zone J.*, *7*(2), 757–768, doi:10.2136/vzj2007.0082.

van Genuchten, M. T. (1980), A closed-form equation for predicting the hydraulic conductivity of unsaturated soils, *Soil Sci. Soc. Am. J.*, *44*(5), 892–898, doi:10.2136/sssaj1980.03615995004400050002x.

Vergnes, J.-P., B. Decharme, and F. Habets (2014), Introduction of groundwater capillary rises using subgrid spatial variability of topography into the ISBA land surface model, *J. Geophys. Res. Atmos.*, *119*, 11,065–11,086, doi:10.1002/2014JD021573.

Vidal, J.-P., E. Martin, L. Franchistéguy, M. Baillon, and J.-M. Soubeyroux (2010), A 50-year high-resolution atmospheric reanalysis over France with the Safran system, *Int. J. Climatol.*, *30*(11), 1627–1644, doi:10.1002/joc.2003.

Weill, S., E. Mouche, and J. Patin (2009), A generalized Richards equation for surface/subsurface flow modelling, *J. Hydrol.*, *366*(1–4), 9–20, doi:10.1016/j.jhydrol.2008.12.007.

White, W. N. (1932), A method of estimating ground-water supplies based on discharge by plants and evaporation from soil—Results of investigations in Escalante Valley, Utah, *Water Supply Pap. 659-A*, USGS Numbered Series, U.S. Dep. of the Inter., Geol. Surv.

Xia, Y. Q., and M. A. Shao (2008), Soil water carrying capacity for vegetation: A hydrologic and biogeochemical process model solution, *Ecol. Model.*, *214*(2–4), 112–124, doi:10.1016/j.ecolmodel.2008.01.024.

Yeh, P. J. F., and E. A. B. Eltahir (2005), Representation of water table dynamics in a land surface scheme: Part I: Model development, *J. Clim.*, *18*(12), 1861–1880, doi:10.1175/JCLI3330.1.

York, J. P., M. Person, W. J. Gutowski, and T. C. Winter (2002), Putting aquifers into atmospheric simulation models: An example from the Mill Creek Watershed, northeastern Kansas, *Adv. Water Resour.*, *25*(2), 221–238, doi:10.1016/S0309-1708(01)00021-5.

Yuan, X., Z. Xie, J. Zheng, X. Tian, and Z. Yang (2008), Effects of water table dynamics on regional climate: A case study over east Asian monsoon area, *J. Geophys. Res.*, *113*, D21112, doi:10.1029/2008JD010180.

Zambrano-Bigiarini, M., and R. Rojas (2013), A model-independent Particle Swarm Optimisation software for model calibration, *Environ. Modell. Software*, *43*, 5–25, doi:10.1016/j.envsoft.2013.01.004.

Zhang, Y., C. Li, C. C. Trettin, H. Li, and G. Sun (2002), An integrated model of soil, hydrology, and vegetation for carbon dynamics in wetland ecosystems, *Global Biogeochem. Cycles*, *16*(4), 1–17.

Zhu, Y., L. S. Shi, L. Lin, J. Z. Yang, and M. Ye (2012), A fully coupled numerical modeling for regional unsaturated-saturated water flow, *J. Hydrol.*, *475*, 188–203, doi:10.1016/j.jhydrol.2012.09.048.